Eur. Phys. J. B **17**, 215–226 (2000)

THE EUROPEAN PHYSICAL JOURNAL B

EDP Sciences

Charge-density-wave instabilities and quantum transport in the monophosphate tungsten bronzes $(PO_2)_4(WO_3)_{2m}$ with m = 5 alternate structure

U. Beierlein[1,a], C. Hess[1], C. Schlenker[1], J. Dumas[1], R. Buder[1], D. Groult[2], E. Steep[3], D. Vignolles[4], and G. Bonfait[5]

[1] Laboratoire d'Études des Propriétés Électroniques des Solides, CNRS, BP 166, 38042 Grenoble Cedex 9, France
[2] ISMRA, Laboratoire CRISMAT, 6 boulevard Maréchal Juin, 14050 Caen Cedex, France
[3] High Magnetic Field Laboratory, MPI-FKF, CNRS, BP 166, 38042 Grenoble Cedex 9, France
[4] Laboratoire de Physique de la Matière Condensée et Service National des Champs Magnétiques Pulsés - INSA, 135 avenue de Rangueil 31077 Toulouse Cedex 4, France
[5] Dept. Quimica, ITN, 2686 Sacavem Codex, Portugal

Received 23 November 1999 and Received in final form 23 March 2000

Abstract. Resistivity, thermoelectric power and magnetotransport measurements have been performed on single crystals of the quasi two-dimensional monophosphate tungsten bronzes $(PO_2)_4(WO_3)_{2m}$ for $m = 5$ with alternate structure, between 0.4 K and 500 K, in magnetic fields of up to 36 T. These compounds show one charge density instability (CDW) at $\approx$ 160 K and a possible second one at $\approx$ 30 K. Large positive magnetoresistance in the CDW state is observed. The anisotropic Shubnikov-de Haas and de Haas-van Alphen oscillations detected at low temperatures are attributed to the existence of small electron and hole pockets left by the CDW gap openings. Angular dependent magnetoresistance oscillations (AMRO) have been found at temperatures below $\approx$ 30 K. The results are discussed in terms of a weakly corrugated cylindrical Fermi surface. They are shown to be consistent with a change of the Fermi surface below $\approx$ 30 K.

PACS. 71.45.Lr Charge-density-wave systems – 72.15.Gd Galvanomagnetic and other magnetotransport effects

1 Introduction

Quasi-two-dimensional (2D) metals often show electronic instabilities. These instabilities can either lead to a Peierls transition to a charge-density-wave (CDW) state, as is the case for some layered transition metal dichalcogenides and some transition metal bronzes and oxides [1,2], or to superconductivity, as for the copper-based high-T_c oxides. To date, the mechanisms that govern which type of instability will take place are not well understood. A study of the family of the quasi two-dimensional conductors, the so-called monophosphate tungsten bronzes with general formula $(PO_2)_4(WO_3)_{2m}$, where m is an integer which can vary between 4 and 14 [3–5], could shed some light on this problem.

Most of the members of this series of compounds have been synthetized more than fifteen years ago [6]. Their lattice is orthorhombic or monoclinic (pseudo-orthorhombic) with pentagonal tunnels. It consists of ReO_3-type infinite layers of WO_6 octahedra parallel to the (**a**, **b**) plane, separated by layers of PO_4 tetrahedra. Since the $5d$ conduction electrons are mainly confined in the center of the WO_6 octahedra layers, the electronic properties are quasi-2D and the Fermi surface is quasi-cylindrical. The thickness of the perovskite WO_6-type slabs and therefore also the **c** parameter, increase with increasing m, whilst **a** and **b** are only weakly m-dependent. It is this property that allows us to vary the low-dimensional character of these compounds and which has a pronounced effect on the Peierls temperatures. There is a clear tendency towards an increase of T_c with increasing m [4]. This may be due to an increase of the low-dimensional character with increasing m. It is reasonable to assume that the conduction electrons in adjacent layers are further apart if the c-parameter is increased. This corresponds to an increase in interlayer distance, which in turn results in a weaker transverse coupling. As a consequence, the Fermi surface becomes more and more cylindrical giving rise to better nesting properties and higher transition temperatures.

The compounds corresponding to $m = 4$ and $m = 6$ have been studied extensively. Two anomalies were observed in the resistivity *versus* temperature curves. They occur at $T_{c_1} = 80$ K and $T_{c_2} = 52$ K for $m = 4$ [7] and at $T_{c_1} = 120$ K and $T_{c_2} = 62$ K for $m = 6$ [8]. X-ray diffuse scattering studies have shown that these anomalies

[a] e-mail: beierlei@lepes.polycnrs-gre.fr

correspond to transitions to incommensurate CDW states [9,10].

Band structure calculations for the normal state using a tight binding extended Hückel method in a 2D approximation have revealed that there are three bands crossing the Fermi level [11]. The Fermi surface (FS) resulting from a superposition of the three FS sheets indicates good nesting properties. This is the so-called hidden nesting or hidden one-dimensionality, caused by the presence of infinite chains of WO_6 octahedra along the **a**, (**a**+**b**) and (**a**−**b**) directions, which correspond to parallel planes on the FS. The calculated band structures for the compounds $m = 4$, $m = 5$ and $m = 6$ differ only slightly.

The $m = 4$ and $m = 6$ compounds show a large positive and anisotropic magnetoresistance in the CDW state at low temperatures [3,12]. Since this magnetoresistance is giant when the magnetic field is perpendicular to the layers, it is attributed to the presence of both hole and electron small quasi-cylindrical FS-pockets with large mobilities and which remain after the CDW gap openings. Quantum transport properties allow us to estimate the size and number of these FS pockets [13]. Thus, FS areas have been determined using Shubnikov-de Haas (SdH) measurements to be roughly 5.4% for $m = 4$ and 1.1% for $m = 6$ of the high temperature two-dimensional Brillouin zone. These results indicate that the $m = 6$ compound has a more pronounced 2D character than the $m = 4$ compound.

The $m = 5$ members of this family were only recently synthetized. This compound has been found to exist in two different varieties. The crystal structure of the first type is built up of a regular stacking of layers corresponding to $m = 5$. This variety will be called "regular structure 5/5". It has been shown using X-ray diffraction measurements that this variety exhibits two successive Peierls transitions at $T_{c_1} = 83$ K and $T_{c_2} = 60$ K [14]. Only one anomaly at ≈ 60 K is detected in transport measurements [15]. The crystal structure of the second type is made up of layers of WO_6 octahedra of different thicknesses: The structure can be viewed as a regular intergrowth of slabs $m = 4$ and $m = 6$ as depicted in Figure 1. This variety will be named "alternate structure 4/6". The alternate structure is the more stable compound of the two varieties. X-ray diffraction studies of the alternate structure have determined a Peierls transition at $T_{c_1} = 158 \pm 2$ K. The critical wave vector **q**, associated with this transition has, within experimental errors, commensurate (**a***, **b***) components. Its intensity shows an anomalous thermal dependence including hysteresis effects [16].

In this article, we present both the classical and quantum transport properties of the compound with alternate structure $m = 4/6$. Resistivity, magnetoresistance and thermoelectric power measurements, as well as Shubnikov-de Haas and de Haas-van Alphen oscillations, have been studied. Further information on the CDW state was obtained through the study of the angular dependent magnetoresistance oscillations (AMRO). The results obtained in the normal and the CDW state are discussed in relation with the quasi two-dimensional FS of this compound and will be compared to the more conventional compounds, $m = 4$ and $m = 6$. We propose that the FS undergoes changes below 30 K. A possible existence of a spin density wave (SDW) state at low temperature is discussed.

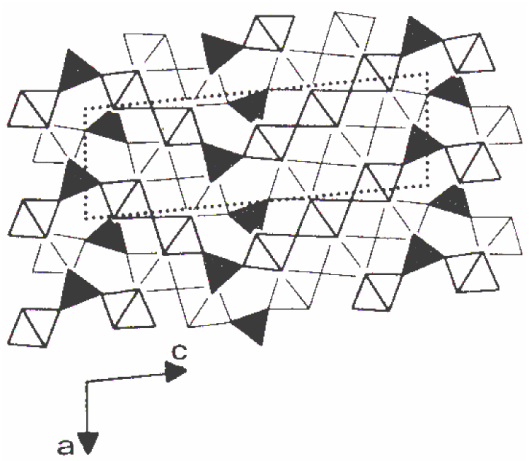

Fig. 1. Crystal structure of $(PO_2)_4(WO_3)_{10}$ with an alternate stacking 4/6 [17].

2 Experimental techniques

Single crystals of $(PO_2)_4(WO_3)_{10}$ with an alternate structure used in these studies were grown using the chemical vapour-transport technique [17]. The crystals are in the form of platelets parallel to the (**a**, **b**) conducting plane, and are of typical size $1.5 \times 0.5 \times 0.3$ mm^3. In order to achieve good electrical contact, it was first necessary to clean the samples. This was carried out by immersing them in ammonia for about half an hour. Four thin silver pads were then evaporated onto the surface of the sample and gold wires (25 μm in diameter) were attached onto the contact pads with silver paste. Contact resistances were typically of a few Ω, three orders of magnitude larger than the sample resistance at 4.2 K. Resistivity and magnetoresistance measurements on selected crystals were carried out using a standard four-probe technique in a He^4 cryostat over a temperature range of 4.2 to 300 K. Measuring currents were in the range 1–5 mA. For the resistance measurements, the electrical current was applied parallel to the (**a**, **b**) plane, whereas for some of the SdH and the AMRO measurements, the current was passed along the **c*** axis.

AMRO are measured by recording the resistance of a crystal of $(PO_2)_4(WO_3)_{10}$ as a function of the angle θ between its crystalline **c*** axis and a constant external horizontal magnetic field. The sample was mounted on a gear-driven rotator. In this way, scans may be performed in different rotational directions. These directions are labeled with an azimutal angle ϕ which describes the plane of rotation. Some of the resistivity measurements

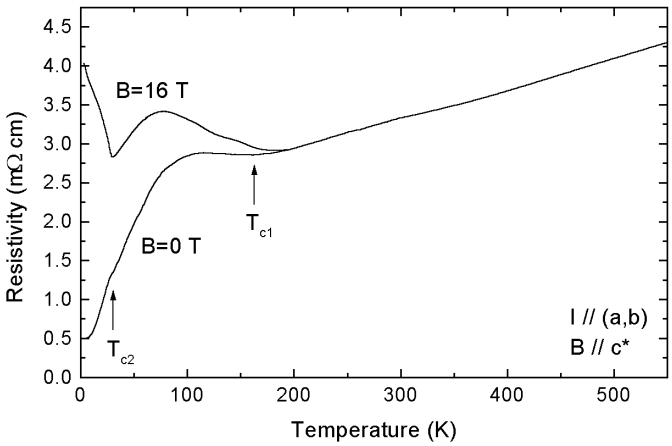

Fig. 2. In-plane resistivity ρ_{ab} of $(PO_2)_4(WO_3)_{10}$ with alternate structure as a function of temperature at $B = 0$ (lower curve) and in a magnetic field of $B = 16$ T (upper curve). The magnetic field is perpendicular to the (**a**, **b**) plane. The inset shows the out-of-plane resistivity $\rho_c(\mathbf{I} \parallel \mathbf{c}^*)$ in zero field.

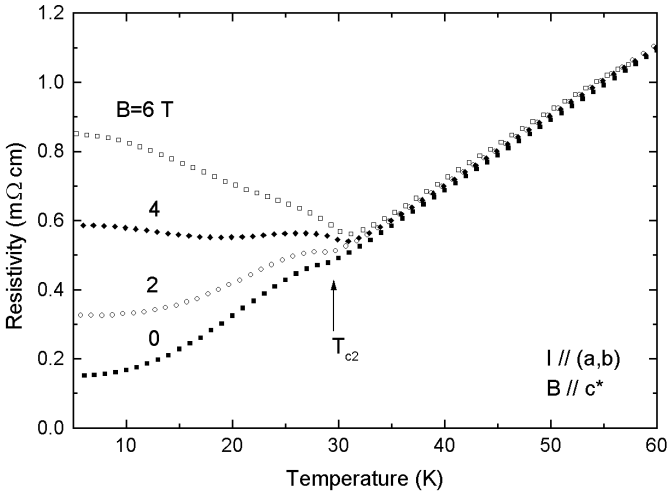

Fig. 3. Low temperature resistivity ρ_{ab} of $(PO_2)_4(WO_3)_{10}$ as a function of temperature in different magnetic fields, B. The current is parallel to the (**a**, **b**) plane and the magnetic field is along $\mathbf{c}^*$.

were made down to 0.05 K using a dilution $He^3 - He^4$ cryostat and a lock-in detection.

The thermopower measurements were performed at temperatures between 6 and 300 K using a slow ac (0.01 Hz) technique similar to that described in reference [18]. The ends of the crystals were fixed by two gold foils and glued with silver paste, ensuring good thermal contact with the heating blocks. The latter were used to apply an alternating temperature gradient ΔT across the sample (ΔT max $\pm$ 1 K). The Seebeck voltage and the corresponding temperature difference, as measured by an Au-Fe thermocouple, were recorded during three measurement cycles, during which the whole setup is kept at a constant temperature. The experiment was entirely computer controlled.

In order to measure the magnetoresistance, the sample was mounted in a He^4 cryostat equipped with a superconducting split-coil which provided fields of up to 8 T. The sample could be rotated about two perpendicular axis with an angular resolution of $\pm 0.1°$ in θ and of $\pm 2°$ in ϕ.

De Haas- van Alphen (dHvA) and Shubnikov- de Haas measurements were carried out at the High Magnetic Field Laboratory (MPI-FKF/CNRS) in Grenoble (France). For the dHvA measurements a capacitive torque method was used. The signal was detected by means of a capacitance bridge. The sample was mounted on a revolving sample holder. Thus, scans over an angular range of $-90° < \theta < 90°$ could be performed. For both dHvA and SdH measurements, a discontinuous He^3-system provides temperatures down to 0.4 K in magnetic fields of up to 28 T, attained by using a hybrid-magnet. SdH measurements were also carried out at SNCMP-Toulouse (France) in pulsed magnetic fields of up to 36 T between 1.6 and 45 K using a contact configuration whereby the current was parallel to the $\mathbf{c}^*$ axis. Other series of SdH measurements were performed at MPI-FKF/CNRS up to 26 T and at ITN Lisbon (Portugal) up to 16 T and 0.3 K using a He^3 cryostat.

3 Experimental results

3.1 CDW instabilities

In this section, we describe the experimental study of the classical transport properties of $(PO_2)_4(WO_3)_{10}$ with alternate structure. Figure 2 displays a typical resistivity curve, measured with the dc current parallel to the (**a**, **b**) plane [19]: At high temperatures, ρ_{ab} is characteristic of a metal with a quasi-linear behavior, whereas at lower temperatures two anomalies are observed. The first is in the vicinity of $T_{c_1} = 160$ K and characterized by a shallow minimum. As the temperature is decreased, it is followed by a bump at ≈ 100 K, then a steep decrease in resistivity at still lower temperature. The second anomaly is seen as a weak kink around $T_{c_2} = 30$ K. The inset to Figure 2 shows the temperature-dependence of the out-of-plane resistivity, ρ_c, *i.e.* when the current is applied parallel to the $\mathbf{c}^*$ axis. The resistivity increases with decreasing temperature and reaches a maximum at ~ 48 K. At lower temperatures, a strong decrease of the out-of-plane resistivity is observed. The anomaly at $T_{c_1} = 160$ K is not seen on this curve, whereas the kink at $T_{c_2} = 30$ K can also be detected in this configuration. The anisotropy of the resistivity ρ_c/ρ_{ab} at 4.2 K is between 40 and 120, depending on the sample's quality. Complementary measurements of the sample's resistivity were carried out at temperatures of down to 0.05 K using a $He^3 - He^4$ dilution cryostat. Metallic conductivity with no sign of superconductivity was detected.

Figure 3 shows the temperature dependence of the resistivity ρ_{ab} at low temperature. The sample was held in magnetic fields of up to 6 teslas perpendicular to the plane of the layers. The onset of a large magnetoresistance at $T_{c_2} = 30$ K is clearly visible.

Resistivity measurements in high magnetic fields of up to 16 T indicate that the magnetoresistance persists

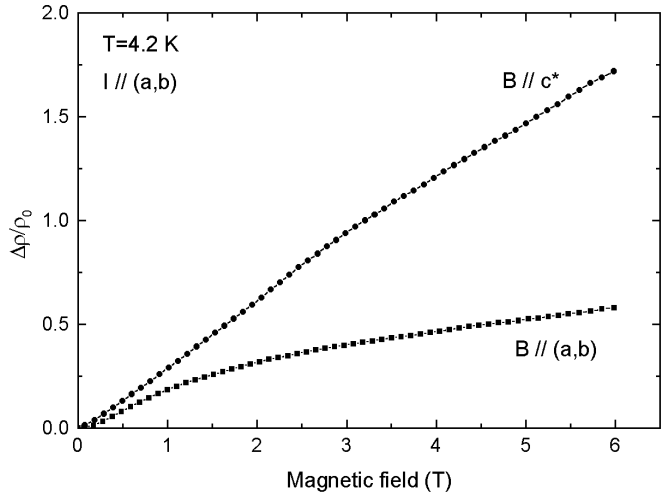

Fig. 4. Transverse magnetoresistance as a function of the magnetic field for B along $\mathbf{c}^*$ and $\mathbf{B}$ in the ($\mathbf{a}$, $\mathbf{b}$) plane at $T = 4.2$ K.

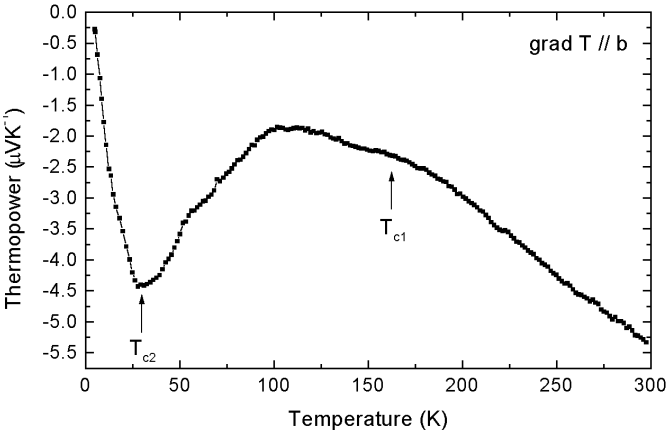

Fig. 5. Thermal variation of the thermoelectric power of $m = 5$ (alternate structure). The temperature gradient is applied along the $\mathbf{b}$ crystallographic axis.

at temperatures as high as 190 K and gradually increases as the temperature is lowered, as depicted in Figure 2. The anomaly at $T_{c_2} = 30$ K appears as an abrupt upturn of the magnetoresistance. Depending on the sample quality, the resistance at 16 T and at $T = 4.2$ K can reach eight times its zero field value. Figure 4 shows the transverse magnetoresistances at $T = 4.2$ K for the magnetic field parallel and perpendicular to the $\mathbf{c}^*$ axis. A strong anisotropy is observed. The magnetoresistance is expressed relative to the zero-field resistivity $\Delta\rho/\rho_0 = (\rho(B) - \rho(0))/\rho(0)$.

The temperature dependence of the thermopower S, is given in Figure 5, measured with the temperature gradient along the ($\mathbf{a}$, $\mathbf{b}$) plane. S is found to be isotropic in this plane. In the high temperature state ($T > T_{c_1}$), S is electron-like. It is negative over the whole temperature range explored. Whilst the transition at T_{c_1}, at about 160 K, is associated with a change of slope, the second transition at 30 K corresponds to a deep local minimum in the $S(T)$ curve. The transition at T_{c_2} coincides with

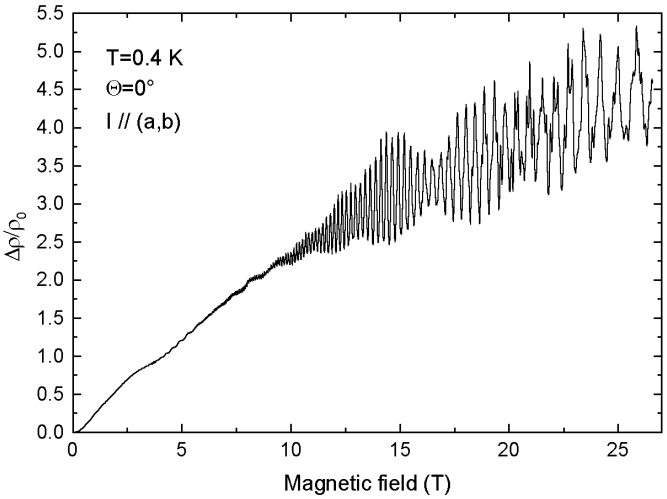

Fig. 6. Transverse magnetoresistance showing quantum oscillations at $T = 0.4$ K. The magnetic field is parallel to the $\mathbf{c}^*$ axis.

a thermopower minimum which may be caused by phonon-drag. Such a minimum often occurs at low temperatures in this class of materials. In the low temperature state (< 10 K), the thermopower is clearly electron-like, which indicates that the electron pockets are dominant.

3.2 Quantum properties

3.2.1 Angular dependence of the quantum oscillation frequencies

Shubnikov-de Haas measurements:

The strong magnetoresistance of the samples is an indication of their high quality. It is this high quality which allows the observation of quantum oscillations. This yields still further information about the CDW state.

Large amplitude SdH oscillations with the magnetic field direction perpendicular to the ($\mathbf{a}$, $\mathbf{b}$) plane at $T = 0.4$ K are shown in Figure 6 [20]. At this temperature, the oscillatory behavior sets in at about 4 T and increases in amplitude as the magnetic field is increased. The oscillatory part of the magnetoresistance is found to be a periodic function of $1/B$. Since the background magnetoresistance is strongly field and temperature dependent, the measured data were divided by the fitted background using a polynomial law for each field-scan. Figure 7 presents the Fourier spectrum of the oscillating part of the curve in Figure 6. At least fifteen distinct peaks can be seen (Tab. 1). In a simple model, one may attribute each of the observed frequencies to an extremal k-space trajectory about the FS in a plane perpendicular to the applied magnetic field [21]. The SdH frequencies are then proportional to the area in k-space of each FS pocket. However, it is also possible that some of the observed frequencies correspond to the second harmonics of lower frequencies. A complete understanding of the origin of each frequency is difficult,

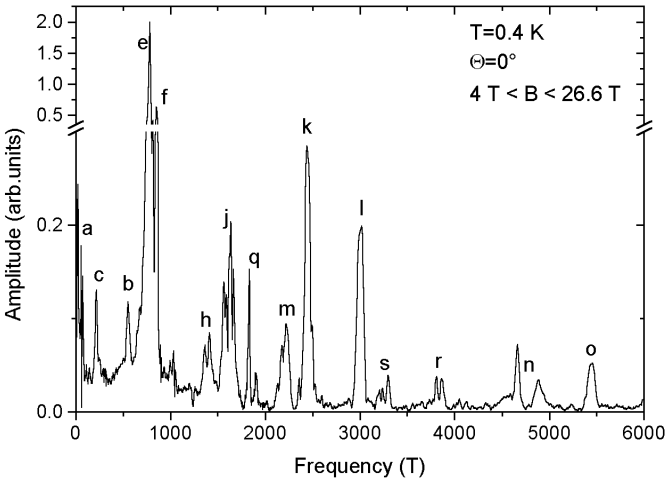

Fig. 7. Fourier transform of the oscillating part of the magnetoresistance for $T = 0.4$ K, performed over the whole field range where the oscillations are detected. The magnetic field is parallel to the $\mathbf{c}^*$ axis.

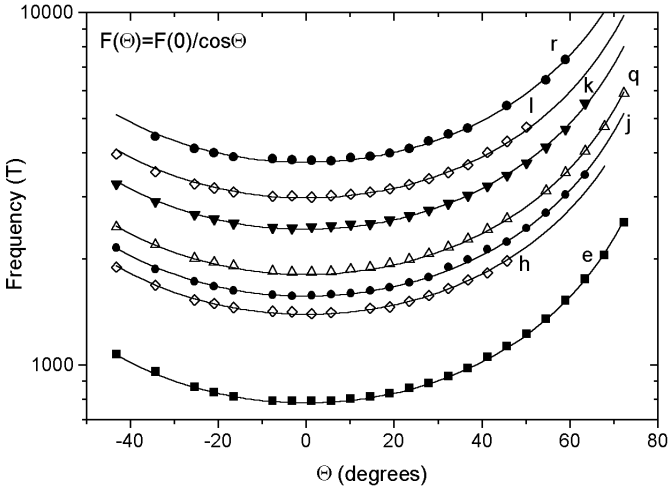

Fig. 8. Angular dependence of the SdH oscillation frequencies at $T = 0.4$ K. The solid lines show the $1/\cos(\theta)$ dependence, where θ is the angle between the applied field and the $\mathbf{c}^*$ axis.

Table 1. Frequencies, effective cyclotron masses for the measured SdH and dHvA oscillations, extremal FS area as a percentage of the high temperature Brillouin zone, Dingle temperatures.

name	Frequency (T)	$\left(\frac{m^*}{m_0}\right)_{\mathrm{SdH}}$	$\left(\frac{m^*}{m_0}\right)_{\mathrm{dHvA}}$	S (% BZ)	T_{D}(K)
a	57	0.32		0.48	
c	210	0.34	0.20	1.8	
e	790	1.1	1.3	6.6	5.3
f	850	1.2		7.1	
h	1 380			11.4	
j	1 600	0.42		13.3	9
q	1 830	0.96	0.92	15.3	
m	2 230			18.7	
k	2 440	1.2	1.1	20.4	3.5-4.5
l	3 000			25.1	
s	3 250	0.55		27.2	
r	3 800	0.54		31.8	
n	4 540			38.0	
o	5 450			45.5	

particularly since the ground-state FS of $(PO_2)_4(WO_3)_{10}$ in the CDW state is not known. However, it is reasonable to assume that most of the frequencies correspond to distinct extremal orbits in k-space. It is also difficult to determine whether each or any of the apparent closed k-space trajectories belong to a single FS pocket or if they result from a combination of two or more pockets through a magnetic breakdown process [22]. Most of the peaks exhibit splitting into two and sometimes three or four peaks. The separation in frequency of the splitted peaks is angle-dependent. For $\theta = 0°$, the difference in frequency of most of the splitted peaks is between 33 and 70 T.

Angular dependent studies of the SdH oscillation frequencies have been performed to check the two-dimensional character of the FS (Fig. 8). It is found that each SdH oscillation frequency follows a $1/\cos(\theta)$ dependence (θ being the angle between the applied field and the $\mathbf{c}^*$ axis). This confirms the existence of multiple cylindrical FS-pockets elongated along the $\mathbf{c}^*$ axis, since, for any direction of the magnetic field, the orbits described by the charge carriers are ellipses. The cross-sections of these ellipses vary as $1/\cos(\theta)$.

For some of the SdH oscillation frequencies, the Dingle temperatures, T_{D}, could be determined by application of the "Dingle" reduction factor, $R_{\mathrm{D}} = \exp\left(-2\pi^2 p m^* k_{\mathrm{B}} T_{\mathrm{D}}/e\hbar B\right)$, given in the Lifshitz-Kosevich theory [21,23]. Values of T_{D} of between 3.5 and 9 K have been found (see Tab. 1). The rates of electronic scattering calculated from these temperatures are in the range of 2.9 to 7.4 $\times 10^{12}$ s^{-1}. These large values of T_{D} correspond to broadened Landau levels with a much more smeared out density of states and a less oscillating chemical potential. This might justify the application of the conventional 3D Lifshitz-Kosevich theory in spite of the quasi two-dimensional character of this material.

de Haas-van Alphen measurements:

de Haas-van Alphen (dHvA) measurements were carried out at $T = 0.4$ K using a capacitive torque method. The magnetic field was varied between 18 and 27 T. The dHvA oscillations were observed for different angles θ between the field direction and the $\mathbf{c}^*$ axis, as depicted in Figure 9. Figure 10 shows the Fourier spectrum of the data for $\theta = 0°$ at $T = 0.4$ K. The observed frequencies are the same as those seen in the Fourier spectrum of the SdH oscillations. For both dHvA and SdH measurements described in this paragraph, the same sample was studied. However, the resolution of the dHvA frequencies is poorer than that of the SdH oscillations, due to the smaller field

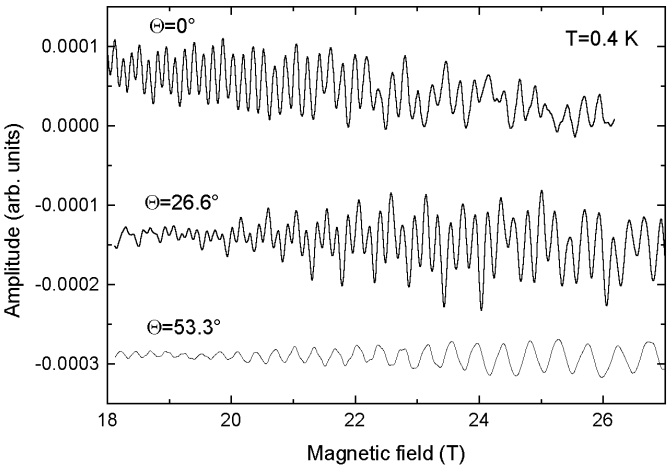

Fig. 9. dHvA torque signal at $\theta = 0°$, 26.6° and 53.3° at $T = 0.4$ K as a function of the magnetic field.

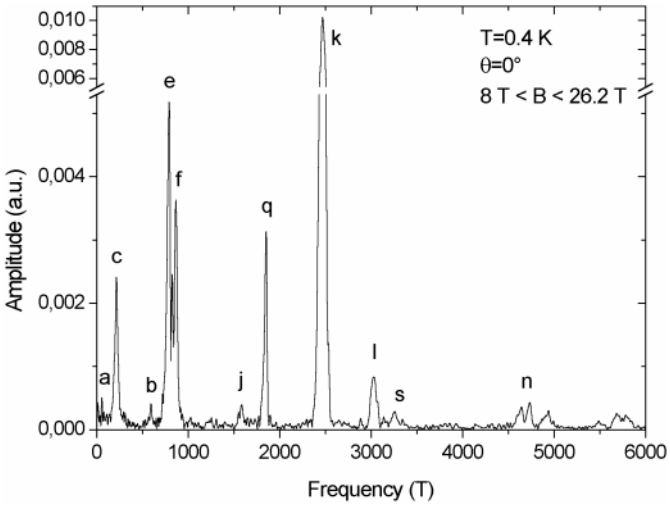

Fig. 10. Fourier transform of the dHvA torque signal at $\theta = 0°$ and at $T = 0.4$ K.

range explored in the dHvA measurements. Note that the ratio of the amplitudes of the peaks is different to the ratio of the SdH amplitudes in the same field range. The angular variation of the dHvA frequencies is presented in Figure 11. The data confirm the $1/\cos(\theta)$ dependence also obtained in the SdH measurements.

3.2.2 Thermal variation of the frequencies' amplitude and relaxation time

We now turn our attention to the temperature dependence of the SdH oscillations. A second series of SdH measurements was performed in pulsed magnetic fields of up to 36 T using another sample of the same material. The temperature was varied between 1.7 and 43 K. The current was applied parallel to the $\mathbf{c}^*$ axis in order to obtain higher resistivity values. The frequency spectrum was not sensitive to the contact configuration or the sample used. Figure 12 presents the magnetoresistance *versus* field of

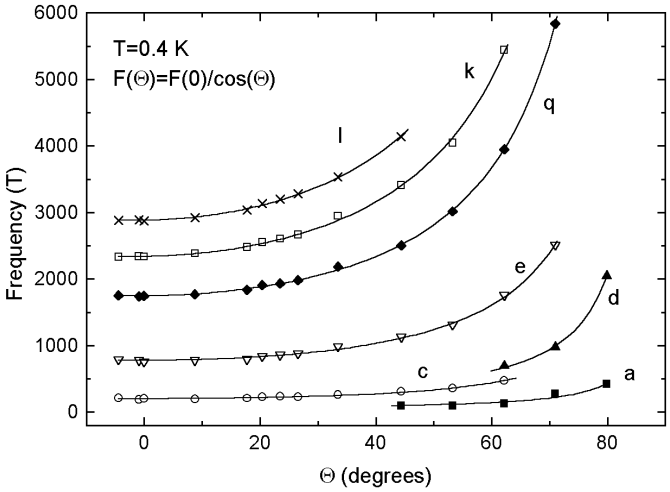

Fig. 11. Angular dependence of the dHvA frequencies. The solid lines are $1/\cos(\theta)$ fits corresponding to a cylindrical FS.

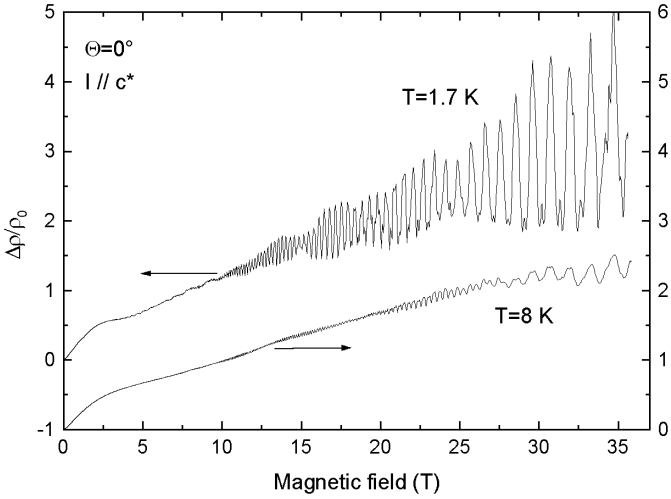

Fig. 12. Magnetic field dependence of the magnetoresistance parallel to the $\mathbf{c}^*$ axis at $T = 1.7$ K and $T = 8$ K. The magnetic field is perpendicular to the (**a**, **b**) plane.

$(PO_2)_4(WO_3)_{10}$ with alternate structure at 1.7 and 8 K. The carrier effective masses may be deduced using the Lifshitz-Kosevich reduction factor, $R_T = xT/\sinh(xT)$, where x is given by: $x = 2\pi^2 pm^* k_B/\hbar eB$. Here, m^* is the cyclotron mass and p is an integer which represents the pth harmonic order of the Fourier spectrum [21]. The relative amplitude of each SdH oscillation is obtained from its Fourier transform peak height. As an example, Figure 13 presents the temperature dependence of the amplitude of three of the frequencies together with a fit according to the Lifshitz-Kosevich formula. Only the two oscillation frequencies, labeled c and j, remain at 20 K. Between 22 K and 24.5 K, oscillation j disappears abruptly. In the same temperature region, oscillation c undergoes a change in slope if its amplitude is plotted according to an effective mass plot (see Fig. 13). Oscillation c was observed at temperatures of up to 43 K. Table 1 summarizes the results of such a fitting procedure for each frequency,

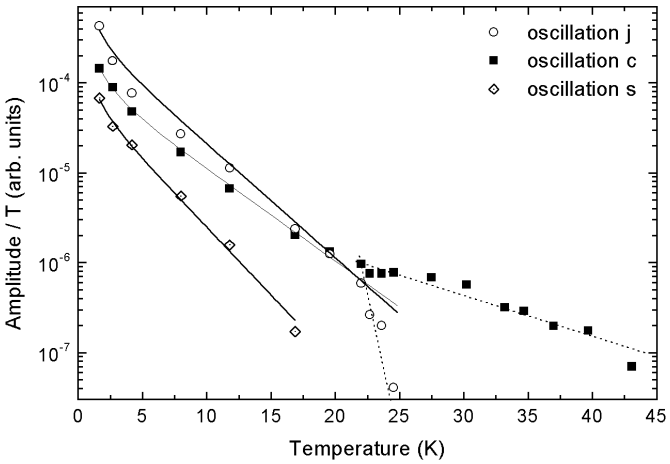

Fig. 13. Amplitudes of the SdH oscillations j, c and s for $\mathbf{B} \parallel \mathbf{c}^*$ as a function of temperature (semi-logarithmic scale). The solid lines are fits to the data using the Lifshitz-Kosevich formula, the dotted lines are guides to the eye.

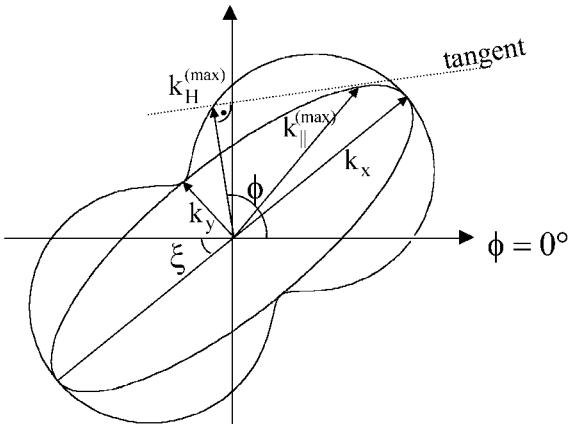

Fig. 14. Schematic look at the transverse cross-section of an elliptical FS. $\mathbf{k}_{||}^{(\max)}$ is the component of the Fermi wave vector in the 2D plane. $k_H^{(\max)}$ is the projection of $\mathbf{k}_{||}^{(\max)}$ along the component of the magnetic field parallel to the 2D plane. k_x and k_y are respectively the major and minor semiaxis of the ellipse which is inclined by an angle ξ with respect to $\phi = 0°$.

together with the results of the same analysis for the dHvA measurements.

3.3 Angular dependent magnetoresistance oscillations

In addition to the SdH oscillations, a new type of oscillation can occur in a quasi two-dimensional conductor at low temperatures, if a weak interlayer interaction between adjacent conducting planes is present [24]. In this case, the cylindrical Fermi surface is warped. The energy dispersion relation of the electrons can be written:

$$\varepsilon_k = \frac{\hbar^2}{2m}(k_x^2 + k_y^2) - 2t_\perp \cos(ck_z) \qquad (1)$$

where k_x and k_y are the x and y components of the wavevector, k, in the conducting plane. $t_\perp$ is the interlayer transfer energy ($t_\perp \ll E_F$) and c is the spacing between adjacent layers. The so-called angular dependent magnetoresistance oscillations (AMRO) are different to the SdH oscillations. They are dependent on the angle θ, but not on the amplitude of the field. Since this phenomenon is essentially a semiclassical effect rather than a quantum effect, AMRO can even be found under conditions whereby no SdH oscillations are detected [25]. In the model proposed by Yamaji [26], the electron velocity normal to the layers, and averaged over all trajectories on the Fermi surface, depends on the magnetic field direction. When the magnetic field direction is such that this averaged electron velocity is equal to zero, the resistance, R, will experience a maximum. This happens periodically as a function of θ, giving rise to AMRO. The maxima in R occur at angles θ_n such that :

$$k_H^{(\max)}\, c \tan\theta_n = \pi\left(n \mp \frac{1}{4}\right) + (\mathbf{k}_{||}^{(\max)} \cdot \mathbf{u}) \qquad (2)$$

where n is an integer. The negative and positive signs correspond to positive and negative θ_n respectively. $\mathbf{k}_{||}^{(\max)}$ is the in-plane component of the Fermi wave vector. The projection of $\mathbf{k}_{||}^{(\max)}$ along the component of the magnetic field parallel to the 2D plane is $k_H^{(\max)}$, as depicted in Figure 14. Also $\mathbf{u}$ is the in-plane part of the direction vector of the interlayer integral [24,27]. If it is assumed that the FS pocket corresponding to the observed AMRO has an elliptical cross section, then the projection vector $k_H^{(\max)}$ is related to the major semiaxis, k_x, and the minor semiaxis, k_y, of the ellipse by

$$k_H^{(\max)} = [k_x^2 \cos^2(\phi - \xi) + k_y^2 \sin^2(\phi - \xi)]^{1/2} \qquad (3)$$

where ϕ is the azimuthal angle describing the angular position in the plane of the ellipse and ξ is the inclination of the major axis with respect to $\phi = 0°$. For an elongated ellipse, equation (3) describes a locus in the form of a figure "eight" in polar $(k_H^{(\max)}, \phi)$ space (Fig. 14) [28]. Thus, by use of equation (3), the shape of the FS can be derived, using a least squares fit to the measured $k_H^{(\max)}$- values.

These oscillations are more apparent in the out-of-plane conductivity. Quasi two-dimensional AMRO are more pronounced when the Fermi surface cylinders are only slightly warped. They have been observed in several quasi two-dimensional conductors [24,28–30] in which they are used in order to map out the FS.

If the electric current is applied parallel to the $\mathbf{c}^*$ axis, also single-crystals of $(PO_2)_4(WO_3)_{10}$ with alternate structure show characteristic resistivity-oscillations as the sample is rotated in a magnetic field. In Figure 15, the temperature dependence of the AMRO of $(PO_2)_4(WO_3)_{10}$ is shown for a field of 7.8 T. At this field, oscillations of the resistivity can clearly be observed at 4.2 K as a function of θ. Thermal damping reduces the oscillation's

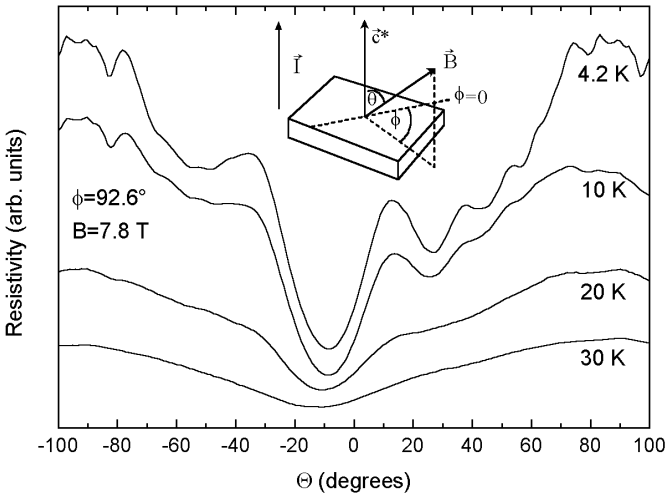

Fig. 15. Temperature dependence of the AMRO in $(PO_2)_4(WO_3)_{10}$ with alternate structure at 7.8 T for $\phi = 92.6°$. θ is defined as the angle between the crystal $\mathbf{c}^*$ axis and the external magnetic field while ϕ is an azimuthal angle in the ($\mathbf{a}$, $\mathbf{b}$) plane.

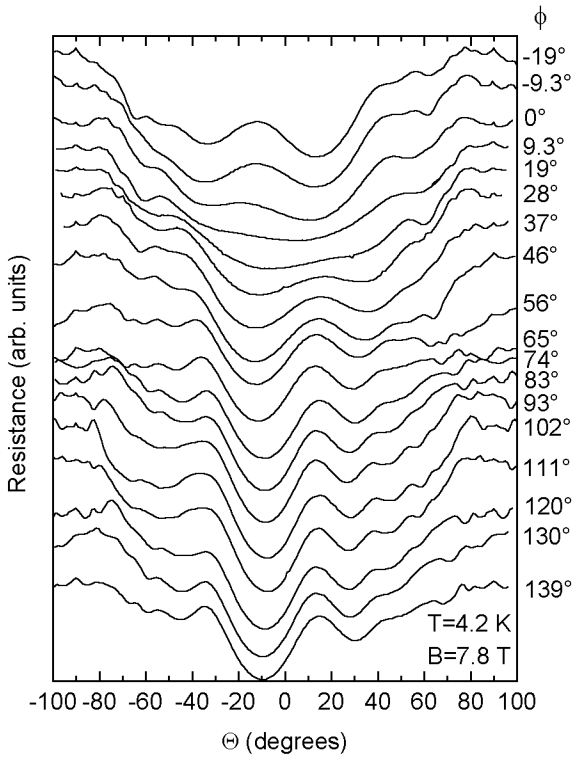

Fig. 16. AMRO in $(PO_2)_4(WO_3)_{10}$ with alternate structure at 4.2 K for several values of ϕ at an applied field of 7.8 T.

amplitude until the AMRO disappear between 20 and 30 K. The positions of the AMRO-peaks do not depend on the applied magnetic field over the field-range explored. In Figure 16, AMRO data at 4.2 K and at 7.8 T are presented for a range of values of ϕ. Although, from a straightforward application of the theory, one might expect a perfect mirror reflection symmetry about $\theta = 0°$, the traces

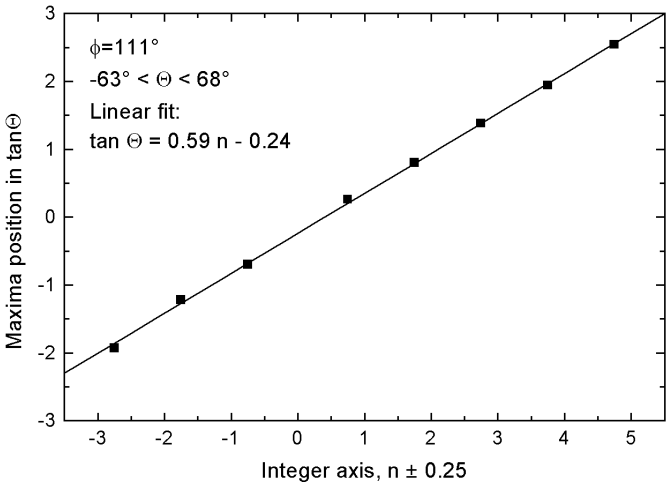

Fig. 17. A fit of the AMRO peak positions to index n for $\phi = 111°$ and $-63° < \theta < 68°$ in 7.8 T.

in Figure 16 are asymmetric about this axis. This could be due to a misalignment of the sample. It should be noted that the orientations of the crystallographic axis in the ($\mathbf{a}$, $\mathbf{b}$) plane are not known for the two samples used in this study. Thus, $\phi = 0$ is an arbitrary direction and does not correspond to any particular direction in the ($\mathbf{a}$, $\mathbf{b}$) plane. The maxima in the magnetoresistance are expected to be periodic in $\tan(\theta)$ at each azimuthal angle ϕ, although the period is a function of ϕ. The projection $k_H^{(\max)}(\phi)$ of the Fermi surface wavevector in the plane of rotation of the magnetic field vector may be deduced from the slope of a plot such as Figure 17, according to equation (2). As an example, Figure 17 shows a linear fit of the AMRO peak positions plotted in $\tan\theta$ as a function of n for $\phi = 111°$. It is clear from equation (2), that this linear dependence will be discontinuous at $\tan\theta = 0°$. This arises, because the difference between the two $\tan(\theta)$ values corresponding to the "-1" and "$+1$" extrema are 1.5 times as large as the period $\Delta(\tan(\theta))$ [31,32]. This discontinuity can be avoided by plotting the positive $\tan(\theta)$ values at $n - 0.25 = 0.75, 1.75, 2.75, \cdots$, and the negative $\tan(\theta)$ values at $n + 0.25 = -0.75, -1.75, -2.75, \cdots$. It should be pointed out that equation (2) is obtained assuming $\tan(\theta) > 1$. However, in our case, the observed AMRO show only slight variations from the linear behavior, even at the lowest angles, for which $\tan(\theta) < 1$.

Values for $k_H^{(\max)}$ could thus be deduced for those directions, ϕ, that the azimuthal angle dependence of the AMRO was recorded. It should be pointed out that only the dominant oscillation could be treated, since oscillations which could correspond to other pockets appearing near 90°, were too weak. This analysis was performed for $-37° < \phi < 250°$. Figure 18 shows the resulting $k_H^{(\max)}$- data points in the ($\mathbf{a}^*$, $\mathbf{b}^*$) plane in polar coordinates. A least squares fit to the data in Figure 18 using equation (3) yielded the major semiaxis of the ellipse, $k_x = (2.59 \pm 0.03) \times 10^9$ m^{-1}, the minor semiaxis, $k_y = (1.61 \pm 0.03) \times 10^9$ m^{-1}, and showed that the major axis is at an angle $\xi = (102 \pm 2)°$ with respect to $\phi = 0°$.

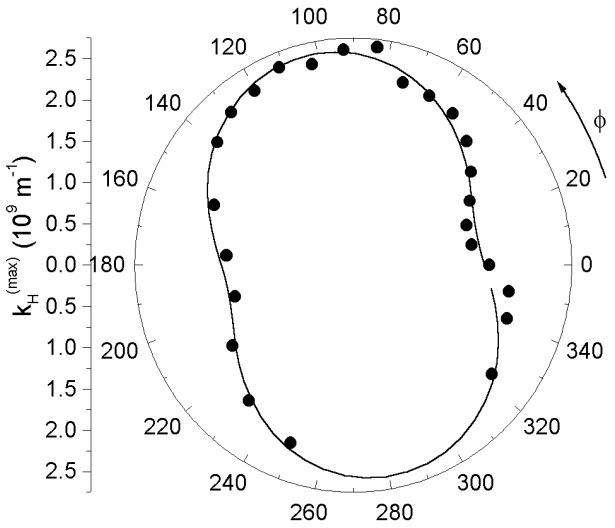

Fig. 18. Projection vector $k_H^{(\max)}$ as a function of ϕ deduced from equation (2) using the measured AMRO data for $-37^\circ < \phi < 250^\circ$. The solid line is a least square fit to equation (3).

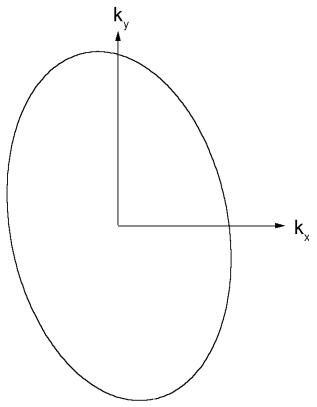

Fig. 19. Resultant cross-section of the FS pocket deduced from AMRO data at 7.8 T and 4.2 K.

The shape of the pocket in cartesian coordinates obtained from this fit is illustrated in Figure 19. The area of the ellipse is thus $S = (13.1 \pm 0.4) \times 10^{18}$ m^{-2} which corresponds to a frequency of $F = (1380 \pm 40)$ T. This is in excellent agreement with the observed SdH oscillation frequency F_h=1380 T which corresponds to 11.4% of the first Brillouin zone area.

4 Discussion

4.1 Charge density wave instabilities

We now treat the normal and the CDW state of $(PO_2)_4(WO_3)_{10}$ with alternate structure, which will be compared with the $m = 4$ and $m = 6$ compounds. Both the in-plane resistivity and thermoelectric power show a quasi linear temperature-dependence in the high temperature metallic state. The in-plane resistivity (at room temperature) is at least one order of magnitude larger than that of the $m = 4$ and $m = 6$ compounds, even though the average number of conduction electrons per tungsten atom is between that of $m = 4$ and $m = 6$. This may be due to a stronger electron-phonon or electron-electron interaction associated with a crystal structure slightly different from that of $m = 4$ or $m = 6$. The temperature-dependence of the out-of-plane resistivity, ρ_c, is completely different. The resistivity along the $\mathbf{c}^*$ axis is non-metallic in behavior ($\mathrm{d}\rho/\mathrm{d}T < 0$) at $T > 50$ K, but becomes metallic-like ($\mathrm{d}\rho/\mathrm{d}T < 0$) below $T < 30$ K. This might be attributed to a crossover between different conduction mechanisms: The metallic behavior at low temperatures may change into a regime that is governed by thermally assisted hopping at higher temperatures. This crossover would occur at about 50 K where the curve ρ_c *vs.* T changes slope. A similar behavior has been reported for 2D superconductors [33].

The resistivity-anomaly at ~ 160 K does not appear as a clear hump, as is the case for the $m = 4$ and $m = 6$ compounds [3], but only as a weak anomaly. This is an indication that the CDW gap or pseudogap-opening only results in a small decrease in the charge-carrier concentration. This shallow minimum in resistivity appears at the temperature at which the thermoelectric power ceases to have a quasi-linear dependence on temperature. The change of slope of $S(T)$ in this temperature region is therefore related to the partial gap opening which modifies the density of states at the Fermi level. Above and below $T_{c1} = 160$ K, the thermoelectric power is negative, which suggests that the electrons are the dominant charge-carriers. X-ray diffraction studies have confirmed the existence of a Peierls transition at $T_{c1} = (158 \pm 2)$ K [16]. The critical wave vector associated with this transition is $\mathbf{q} = (0.33(2); 0.33(2); 0)$ [34]. For the ($\mathbf{a}^*$, $\mathbf{b}^*$) plane components, this is close to the nesting vector corresponding to the first and second transitions in $m = 4$ and $m = 6$ respectively. Such a critical wave vector would simultaneously couple two pairs of parallel sheets on the FS, giving rise to good nesting properties. However, the Peierls transition in this $m = 5$ compound occurs at much higher temperatures than those of the $m = 4$ and $m = 6$ compounds. This higher transition temperature could be a result of a charge transfer between two adjacent layers, one corresponding to $m = 4$ and the other corresponding to $m = 6$, leading to different nesting conditions. The non-monotonous variation of the satellite intensity with temperature seen in X-ray diffraction measurements is consistent with this interpretation [16].

Unlike the $m = 5$ compound with regular stacking, the $m = 5$ compound with *alternate* structure does not have Peierls transitions at temperatures in between those of the $m = 4$ and the $m = 6$ compound.

The second anomaly at ~ 30 K is seen as a kink on both the in-plane and out-of-plane resistivity curves. The minimum in the thermoelectric power at ~ 30 K could be associated with the anomaly detected in the resistivity curve. It may, however, also be the result of a phonon drag mechanism. X-ray diffraction studies performed at temperatures down to 25 K did not show any sign for

a Peierls transition at 30 K. Nevertheless, our study provides strong experimental evidence of a transition in this temperature range, and this is further supported by the observed transport properties of the sample under magnetic field.

4.2 High-field transport properties

4.2.1 Classical transport

As with most of the members of this family of compounds, the low temperature modulated state of $m = 5$ with alternate structure is characterized by a large positive magnetoresistance. When a magnetic field of 16 T is applied, this large magnetoresistance appears at ~ 180 K, near the high temperature transition. This indicates that this compound is a nearly compensated metal in the CDW state. The partial destruction of the FS leaves small quasi-cylindrical electron and hole pockets with high mobilities. The thermoelectric power is always negative, thus electron-type pockets dominate. The pronounced kink seen at ~ 30 K in the resistivity measured in a large magnetic field (16 T) suggests a modification of the FS with a possible spin density wave.

4.2.2 Quantum oscillations

Unlike the $m = 4$ and $m = 6$ compounds, in which only two distinct oscillation frequencies are detected, a great number of frequencies are observed in the $m = 5$ compound. This indicates that the nesting in $m = 5$ results in a less effective destruction of the FS. The FS in the CDW state consists of several cylindrical pockets of different sizes. However, not all of the observed frequencies can correspond to pockets on the FS, since a simple addition of all the pockets' cross-sections gives more than 100% of the high temperature Brillouin zone. Some frequencies could be attributed to the harmonics of lower frequencies, but in this case, the effective masses should also be additive, *e.g.* the first harmonic should have twice the mass of its fundamental frequency. This could not be confirmed for any of the frequencies. Other mechanisms must be considered as being the origin of most of the frequencies.

Since all of the frequencies are observed in both SdH and dHvA measurements, the Stark-effect [21,35] can be excluded as a possible source of oscillations. It is also rather unlikely that an oscillating chemical potential could play a role, since a three-dimensional description of the quantum oscillations using the Lifshitz-Kosevich theory seems to be appropriate [21,36]. This is confirmed by the relatively high Dingle temperatures. Furthermore, the angular variation of the oscillations' amplitudes indicates that spin-splitting [21] is present, but this effect should not produce extra frequencies. However, we suggest that magnetic breakdown leads to combinations of two or more FS pockets, resulting in additional oscillation frequencies. This is supported by the fact that most of the frequencies appear above 10 T. One cannot exclude a deformation of the FS by high magnetic fields.

Taking into account that below 8 T, only the frequencies a, e, j and q can be observed, we suggest that only these frequencies are characteristic of the FS. If this is the case, the total area of the section of the FS pockets would be roughly 36% of the high temperature Brillouin zone section.

The angular variation of the SdH and dHvA oscillation frequencies clearly confirms the quasi two-dimensional character of this material. The splitting of the peaks in the Fourier spectrum is very likely to be caused by a warping of the FS in the $\mathbf{c}^*$ direction. This corrugation of the FS cylinders is a consequence of the weak dispersion in the third spacial direction, *i.e.* perpendicular to the layers. The oscillation frequencies seen in the SdH and dHvA effect are proportional to the extremal cross-section of the FS. Therefore, when measuring a metal with a warped FS, two slightly different frequencies with resulting beating behavior will be observed. Depending on the direction of the applied magnetic field, the frequency dependence will, however, change [24]. A consequence of this is an angular dependent splitting of the quantum transport Fourier peaks and the occurrence of AMRO. This splitting, measured in a magnetic field perpendicular to the ($\mathbf{a}$, $\mathbf{b}$) plane, can be used to estimate the transfer integral perpendicular to the layers, $t_\perp$, using Yamaji's formula [26] for the maximum frequency difference, ΔF_0 of a split peak:

$$\Delta F_0 = \frac{4m^* t_\perp}{e\hbar}.$$

A simple estimation of the transfer integral parallel to the ($\mathbf{a}$, $\mathbf{b}$) plane would be:

$$t_\parallel \sim W \sim \frac{\hbar^2 k_{\mathrm{F}}^2}{2m^*} \sim \frac{\hbar^2 S}{2m^* \pi} \sim \frac{\hbar e F}{m^*}$$

where S is the area of an extremal FS cross-section normal to B and F is the corresponding oscillation frequency. The ratio of the two transfer integrals gives:

$$\frac{t_\perp}{t_\parallel} \sim \frac{\Delta F_0}{4F}.$$

For example, the oscillation denoted h, of frequency $F_h = 1380$ T, and with a separation of the peaks of $\Delta F_0 = 35$ T, when the field is parallel to $\mathbf{c}^*$, yields $t_\perp/t_\parallel \sim 6 \times 10^{-3}$. Values of the same order of magnitude are found for the other oscillation frequencies. This indicates a very weak corrugation of the FS cylinders and a highly two-dimensional character of this compound. This implies a conductivity anisotropy $\sigma_c/\sigma_{ab} \sim (t_\perp/t_\parallel)^2 \sim 3.6 \times 10^{-5}$. However, the anisotropy of the resistivities parallel and perpendicular to the $\mathbf{c}^*$ axis, ρ_c/ρ_{ab}, is between 40 and 120. This might reflect the important role of crystal defects in the conduction mechanisms. Similar discrepancies have been observed in organic low-dimensional materials and have been attributed to incoherent interlayer transport [37].

The effective cyclotron masses associated with each SdH or dHvA oscillation can be determined using

the temperature dependence of the peaks in the Fourier spectrum. Values of between 0.3 and 1.3 free electron masses are obtained. SdH and dHvA measurements are in good agreement. These values are in the same range as the effective masses obtained in the $m = 6$ compound ($m^* \sim 0.3\ m_0$) [38] and in some of the molybdenum bronzes [39,40]. These effective masses are rather light when compared to those obtained in most organic two-dimensional materials and lead to the observation of quantum oscillations at relatively high temperatures.

The Dingle estimated temperatures, deduced from the field dependence of the SdH oscillations, are comparable to those obtained for $m = 6$ ($T_{D_{m=6}} = 8$ K). They are significantly higher than the Dingle temperatures of organic two-dimensional compounds, for which in most cases $T_D < 1$ K [41,42].

The temperature dependence of the oscillations' amplitudes has also shown that one of the SdH oscillation frequencies j, abruptly disappears at $\sim$ 25 K. The remaining oscillation, c, exhibits a change of slope in the effective mass plot at the same temperature. This, and the observed anomalies on the resistivity- and magnetoresistance-curves in this temperature region lead us to the conclusion that the FS undergoes a change in the temperature region between 25 and 30 K. Such modifications of the FS could be induced by a second Peierls transition into a CDW or a spin density wave state. Further X-ray diffraction studies, at still lower temperatures, are required to clarify the nature of this transition.

4.2.3 Angular dependent magnetoresistance oscillations

The study of AMRO provides information on the shape of the FS. At $T = 4.2$ K, and in a magnetic field of 7.8 T, it was possible to determine the shape of one of the FS pockets from the observed AMRO. The AMRO data indicated that this FS pocket is significantly non-circular. The area of the pocket derived from these measurements, compared with the value obtained from the frequency of the corresponding SdH oscillation, revealed that this SdH frequency has a rather weak amplitude and disappears rapidly with increasing temperature. This suggests that this particular FS pocket is only weakly, but regularly corrugated. The ratio of the transfer integrals, derived from the SdH measurements, is small and therefore consistent with this explanation. Strong and irregular corrugations of the FS cylinder represent rather unfavorable conditions for the appearance of AMRO. This could be the reason why the other frequencies that are present in the SdH and dHvA oscillations, are not detected in the AMRO measurements, under the conditions described above. Thermal damping reduces the amplitude of the AMRO until they disappear at temperatures between 20 and 30 K. This can not clearly be linked to a possible Peierls transition in this temperature range. It is possible that the observed pocket dominates the classical transport properties.

5 Conclusions

We have carried out a study of resistivity, thermoelectric power and magnetotransport on single crystals of the quasi two-dimensional CDW conductor $(PO_2)_4(WO_3)_{2m}$ for $m = 5$ with alternate structure. The availability of high quality crystals has enabled a large number of studies of SdH and dHvA oscillations. Information on the Fermi surface in the low CDW state have been obtained. The angular dependences of the SdH and dHvA frequencies follow the $1/\cos(\theta)$ behavior expected for an ideal 2D cylindrical Fermi surface. On the other hand, angular dependent magnetoresistance oscillations (AMRO) have been observed below $\sim$ 30 K. We have shown that they arise from closed orbits on a warped Fermi surface. A Fermi surface shape has been mapped out from AMRO whose area can account satisfactorily for one frequency of the SdH oscillations. Resistivity and magnetoresistance measurements together with an anomalous temperature dependence of the SdH frequencies strongly suggest that a Fermi surface change occurs below 30 K. It would be desirable to study the nature of the phase below 30 K by structural studies.

One of us (U.B.) is grateful to Ministère de l'Éducation Nationale, de L'Enseignement Supérieur et de la Recherche for fellowship. The authors wish to thank P. Foury, E. Canadell, E. Sandré, P. Labbé and I. Wagner for useful discussions. We also acknowledge J.L. Tholence for his help in the very low temperature measurements.

References

1. *Low Dimensional Electronic Properties of Molybdenum Bronzes and Oxides*, edited by C. Schlenker (Kluwer Acad. Publ., Dordrecht, 1989).
2. M. Greenblatt, Int. J. Mod. Phys. B **7**, 4045 (1993).
3. see in *Physics and Chemistry of Low Dimensional Inorganic Conductors*, edited by C. Schlenker, J. Dumas, M. Greenblatt, S. van Smaalen, NATO ASI Series B, Vol. **354** (Plenum, 1996).
4. C. Schlenker, C. Hess, C. Le Touze, J. Dumas, J. Phys. I France **6**, 2061 (1996); J. Dumas, U. Beierlein, S. Drouard, C. Hess, D. Groult, Ph. Labbé, P. Roussel, G. Bonfait, E. Gomez Marin, C. Schlenker, J. Solid State Chem. **147**, 320 (1999).
5. C. Hess, C. Schlenker, J. Dumas, M. Greenblatt, Z.S. Teweldemedhin, Phys. Rev. B **54**, 4581 (1996).
6. J.P. Groult, M. Goreaud, Ph. Labbé, B. Raveau, Acta Cryst. B **37**, 2139 (1981); A. Benmoussa, Ph. Labbé, J.P. Groult, B. Raveau, J. Solid State Chem. **44**, 318 (1982); Ph. Labbé, M. Goreaud, B. Raveau, J. Solid State Chem. **61**, 324 (1986); M. Borel, M. Goreaud, A. Grandin, Ph. Labbé, A. Leclaire, B. Raveau, Eur. J. Solid Inorg. Chem. **28**, 93 (1991).
7. Z.S. Teweldemedhin, K.V. Ramanujachary, M. Greenblatt, Phys. Rev. B **46**, 7897 (1992).
8. E. Wang, M. Greenblatt, I.E. Rachidi, E. Canadell *et al.*, Phys. Rev. B **39**, 12969 (1989).

9. P. Foury, J.P. Pouget, E. Wang, M. Greenblatt, Europhys. Lett. **16**, 485 (1991).
10. A. Ottolenghi, P. Foury, J.P. Pouget, Z.S. Teweldemedhin, M. Greenblatt, D. Groult, J. Marcus, C. Schlenker, Synth. Met. **70**, 1301 (1995).
11. E. Canadell, M. Whangbo, Phys. Rev. B **43**, 1894 (1990).
12. A. Rötger, J. Lehmann, C. Schlenker, J. Dumas, Z.S. Teweldemedhin, M. Greenblatt, Europhys. Lett. **25**, 23 (1994).
13. C. Le Touze, G. Bonfait, C. Schlenker, J. Dumas, M. Almeida, M. Greenblatt, Z.S. Teweldemedhin, J. Phys. I France **5**, 437 (1995).
14. P. Roussel, P. Foury-Leylekian, B. Domengès, D. Groult, Ph. Labbé, J.P. Pouget, Eur. Phys. J. B **12**, 497 (1999).
15. U. Beierlein, C. Schlenker, J. Dumas, D. Groult, Ph. Labbé, E. Balthes, E. Steep, Synth. Met. **103**, 2593 (1999).
16. P. Foury, P. Roussel, D. Groult, J.P. Pouget, Synth. Met. **103**, 2624 (1999).
17. B. Domengès, F. Studer, B. Raveau, Mat. Res. Bull. **18**, 669 (1983).
18. P.M. Chaikin, J.F. Kwak, Rev. Sci. Instrum. **46**, 218 (1975).
19. C. Hess, C. Le Touze, C. Schlenker, J. Dumas, D. Groult, Synth. Met. **86**, 2157 (1997).
20. U. Beierlein, J. Dumas, C. Schlenker, D. Groult, Ph. Labbé, E. Balthes, E. Steep, G. Bonfait, *Int. Workshop on Electronic Crystals ECRYS'99, La Colle sur Loup France, June 1999*, J. Phys. France IV **9**, Pr10-375 (1999).
21. see in D. Shoenberg, *Magnetic Oscillations in Metals* (Cambridge Univeristy Press, Cambridge, 1984).
22. L.M. Falicov, P.R. Sievert, Phys. Rev. **138**, A88 (1965).
23. E.M. Lifshitz, A.M. Kosevich, J. Phys. Chem. Sol. **4**, 1 (1958).
24. J. Wosnitza, *Fermi Surfaces of low-dimensional organic Solids and Superconductors* (Springer Verlag, Heidelberg, 1996).
25. R. Yagi, Y. Iye, T. Osada, S. Kagoshima, J. Phys. Soc. Jpn **59**, 9, 3069 (1990).
26. K. Yamaji, J. Phys. Soc. Jpn **58**, 5, 1520 (1989).
27. M.V. Kartsovnik, V.N. Laukhin, S.I. Pesotskii, I.F. Schegolev, V.M. Yakovenko, J. Phys. I France **2**, 89 (1992).
28. A.A. House, S.J. Blundell, M.M. Honold, J. Singleton, J.A.A.J. Perenboom, W. Hayes, M. Kurmoo, P. Day, J. Phys. Condens. Matter **8**, 8829 (1996).
29. see *e.g.* J. Caulfield, S. J. Blundell, M.S.L. Croo de Jongh, P.T.J. Hendriks, J. Singleton, M. Doporto, F.L. Pratt, J.A.A.J. Perenboom, W. Hayes, M. Kurmoo, P. Day, Phys. Rev. B **51**, 13, 8325 (1995); M.V. Kartsovnik, V.N. Laukhin, J. Phys. I France **6**, 1753 (1996).
30. M. Kawamura, A. Endo, M. Hirasawa, S. Katsumoto, Y. Iye, Physica B **249-251**, 882 (1998).
31. M.V. Kartsovnik, V.N. Laukhin, J. Phys. I France **6**, 1753 (1996).
32. M.V. Kartsovnik, A.E. Kovalev, V.N. Laukhin, S.I. Pesotskii, J. Phys. I France **2**, 223 (1992).
33. K. Yoshida, Y. Maeno, S. Nishizaki, S. Ikeda, T. Fujita, J. Low Temp. Phys. **105**, 1593 (1996).
34. P. Foury (private communication).
35. N. Harrison, D.W. Hall, R.G. Goodrich, J.J.Vuillemin, Z. Fisk, Phys. Rev. Lett. **81**, 870 (1998).
36. N. Harrison, Phys. Rev. Lett. **83**, 1395 (1999).
37. R.H. McKenzie, P. Moses, Phys. Rev. Lett. **81**, 4492 (1998).
38. C. Le Touze, L.H. Nguyen, C. Schlenker, E. Steep, M. Greenblatt, Synth. Met. **86**, 2133 (1997).
39. A. Rötger, C. Schlenker, J. Dumas, J. Wang, Z.S. Teweldemedhin, M. Greenblatt, Synth. Met. **55-57**, 2670 (1993); A. Rötger, J. Lehmann, C. Schlenker, J. Dumas, J. Marcus, Z.S. Teweldemedhin, M. Greenblatt, Europhys. Lett. **25**, 23 (1994).
40. X. Qin, J. Shi, H. Gong, M. Tian, J. Wei, H. Chen, D. Tian, Phys. Rev. B **53**, 15538 (1996).
41. D. Beckmann, S. Wanka, J. Wosnitza, J.A. Schlueter, J.M. Williams, P.G. Nixon, R.W. Winter, G.L. Gard, J. Ren, M.-H. Whangbo, Eur. Phys. J. B **1**, 295 (1998).
42. F.A. Meyer, E. Steep, W. Biberacher, P. Christ, A. Lerf, A.G.M. Jansen, W. Joss, P. Wider, K. Andres, Europhys. Lett. **32**, 681 (1995).